Supporting Information

Ultrafast Rechargeable Zinc Battery Based on High Voltage Graphite Cathode and Stable Nonaqueous Electrolyte

Ning Zhang,[*,†,§] *Yang Dong,*[†] *Yuanyuan Wang,*[†] *Yixuan Wang,*[†] *Jiajun Li,*[†] *Jianzhong Xu,*[*,†] *Yongchang Liu,*[*,‡,§] *Lifang Jiao,*[§] *and Fangyi Cheng*[§]

†College of Chemistry & Environmental Science, Key Laboratory of Analytical Science and Technology of Hebei Province, Hebei University, Baoding 071002, China

‡Beijing Advanced Innovation Center for Materials Genome Engineering, Institute for Advanced Materials and Technology, University of Science and Technology Beijing, Beijing 100083, China

§Key Laboratory of Advanced Energy Materials Chemistry (Ministry of Education), College of Chemistry, Nankai University, Tianjin 300071, China

Corresponding Authors

*(N.Z.) E-mail: ningzhang@hbu.edu.cn; *(J.Z.X.) E-mail: xujz@hbu.edu.cn;

*(Y.C.L.) E-mail: liuyc@ustb.edu.cn

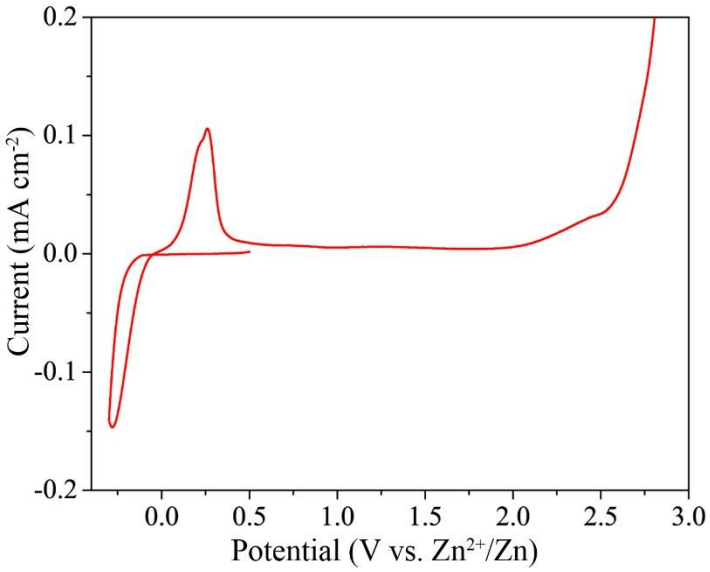

Figure S1. Electrochemical window of the 1 M $Zn(TFSI)_2$ in EC/DEC electrolyte at a scan rate of 1 mV s^{-1}.

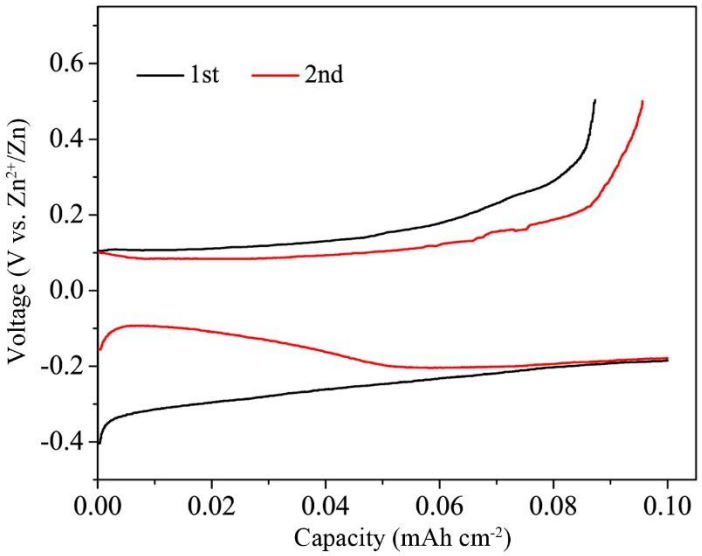

Figure S2. The typical Zn plating/stripping profiles at the 1st and 2nd cycles of the Zn/Ti cell at 0.2 mA cm^{-2} with a deposition capacity of 0.1 mAh cm^{-2}.

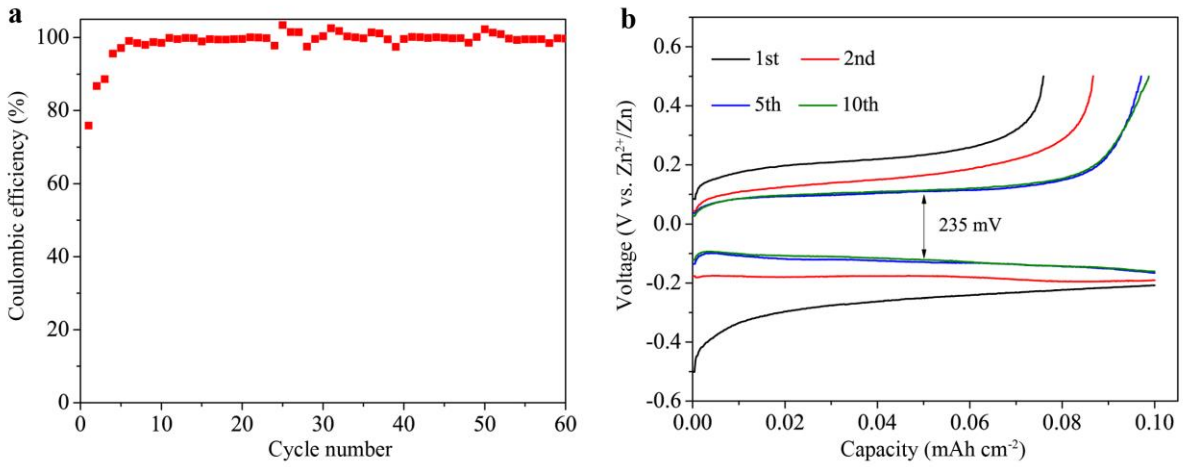

Figure S3. (a) Coulombic efficiency and (b) typical Zn plating/stripping profiles of the Zn/Ti cell using the 1 M $Zn(TFSI)_2$ in EC/DEC electrolyte at 0.2 mA cm^{-2} with a deposition capacity of 0.1 mAh cm^{-2}.

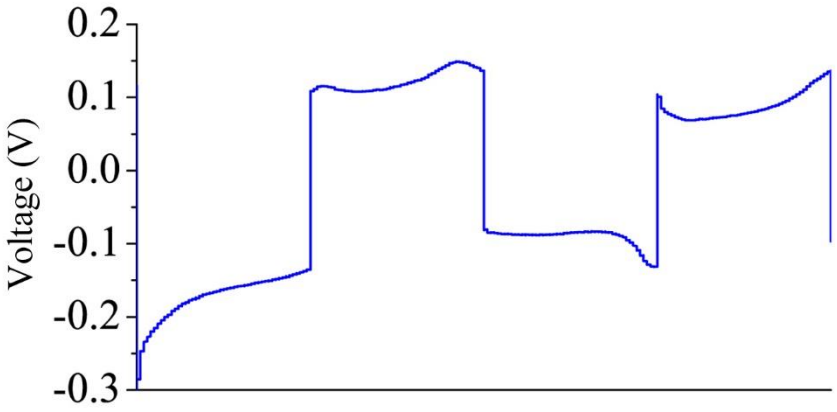

Figure S4. The Zn plating/stripping curves at the initial two cycles of the Zn/Zn symmetrical cell at 0.5 mA cm^{-2} with a discharge/charge time of 0.5 h.

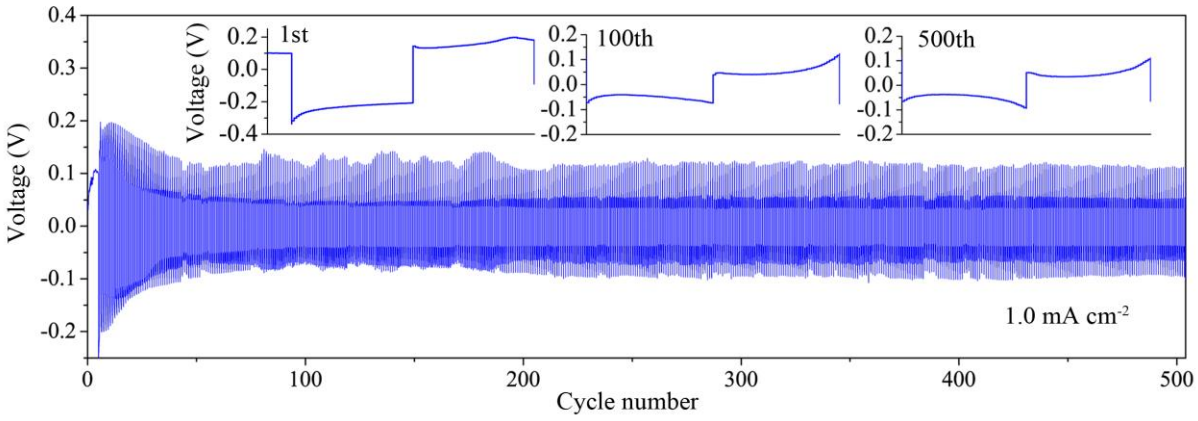

Figure S5. Galvanostatic cycling at 1.0 mA cm^{-2} (discharge/charge time: 0.5 h) of the Zn/Zn symmetrical cell with the selected Zn plating/stripping curves (insets).

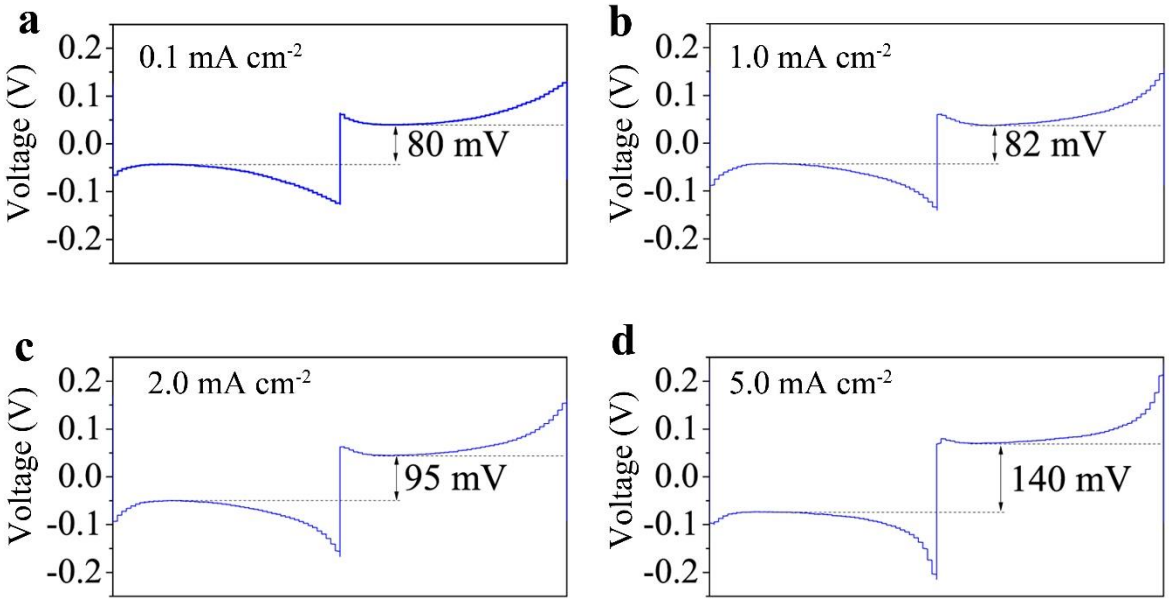

Figure S6. Zn plating/stripping curves of the Zn/Zn cell using 1 M $Zn(TFSI)_2$ in AN electrolyte at (a) 0.1, (b) 1.0, (c) 2.0, (d) 5.0 mA cm^{-2}.

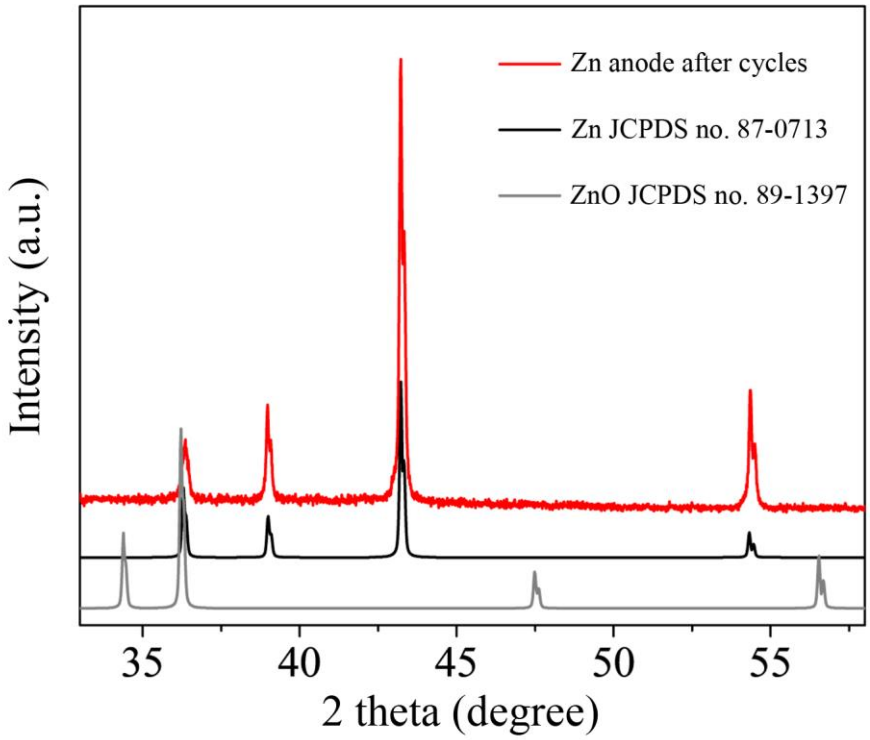

Figure S7. XRD pattern of the Zn anode after 200 cycles.

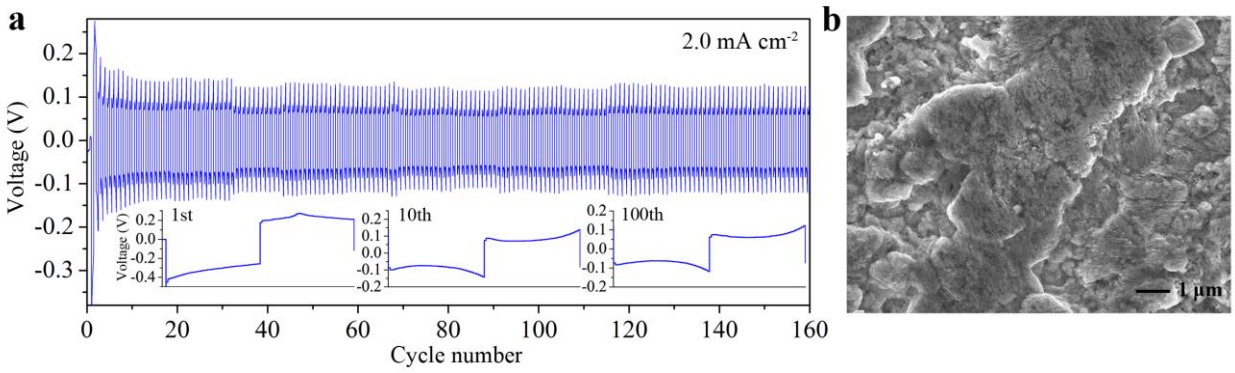

Figure S8. (a) Galvanostatic cycling at 2.0 mA cm^{-2} of the Zn/Zn symmetrical cell with a discharge/charge time of 0.5 h. Insets show the selected Zn plating/stripping curves. (b) SEM image of the Zn anode after 160 cycles.

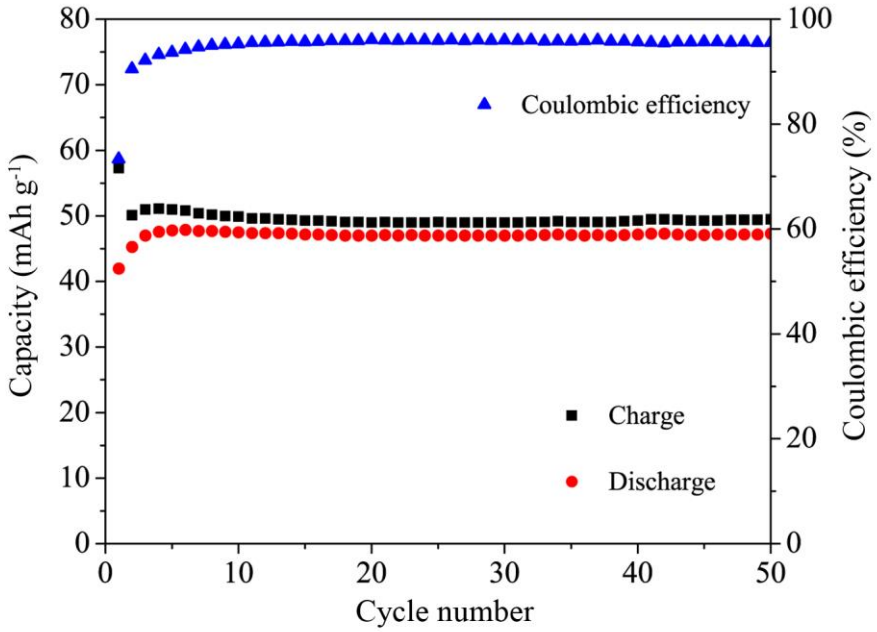

Figure S9. Cycling performance of the Zn-graphite battery using the 1 M $Zn(TFSI)_2$ in AN electrolyte at 50 mA g^{-1}.

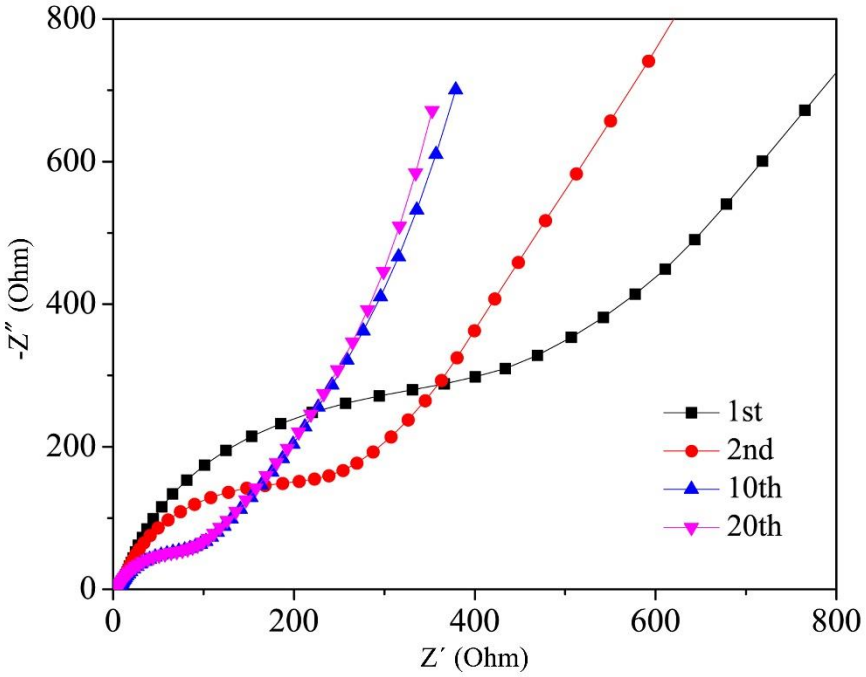

Figure S10. EIS spectra of the Zn-graphite battery after the 1st, 2nd, 10th, and 20th cycles.

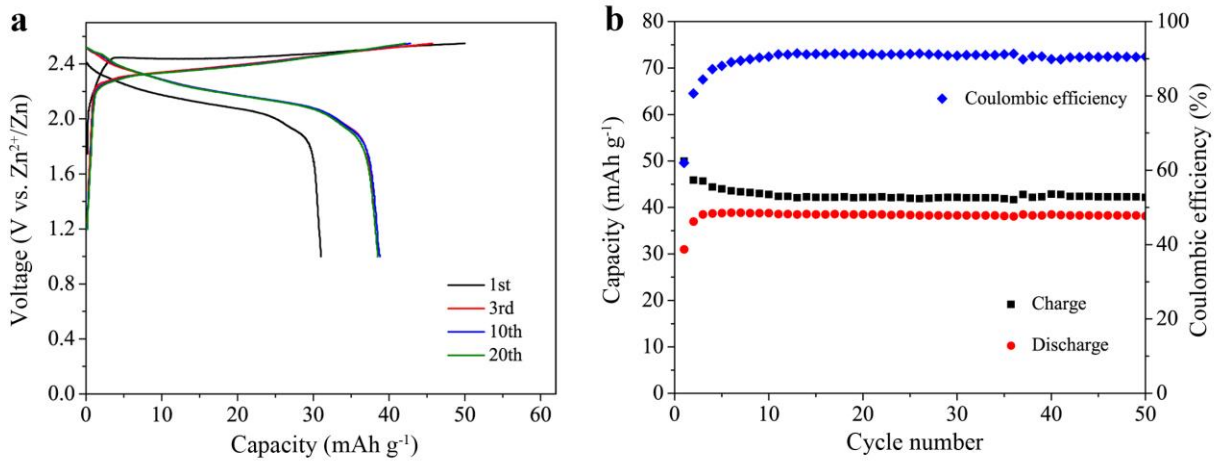

Figure S11. (a) Typical charge/discharge curves and (b) cycling performance at 50 mA g^{-1} of the Zn-graphite battery using the 0.5 M $Zn(TFSI)_2$ in AN electrolyte.

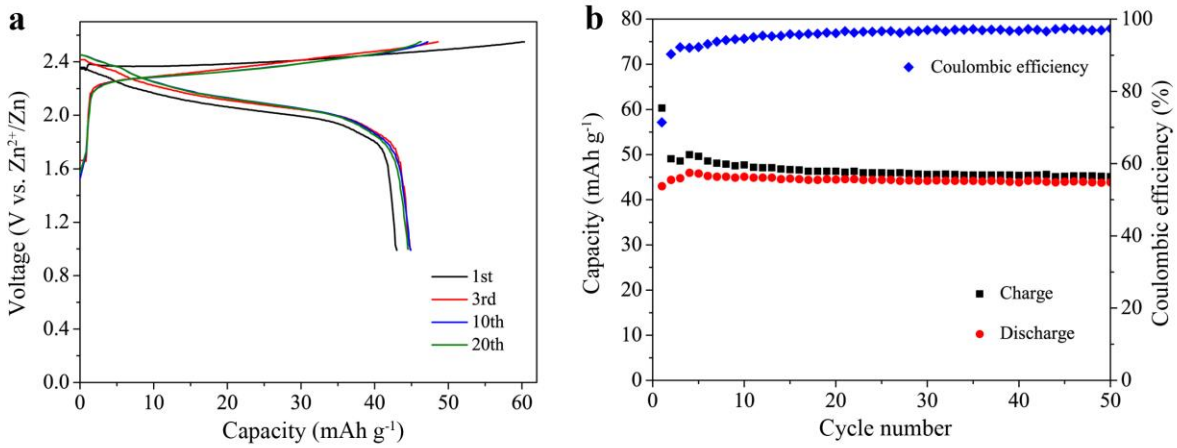

Figure S12. (a) Typical charge/discharge curves and (b) cycling performance at 50 mA g^{-1} of the Zn-graphite battery using the 2 M $Zn(TFSI)_2$ in AN electrolyte.

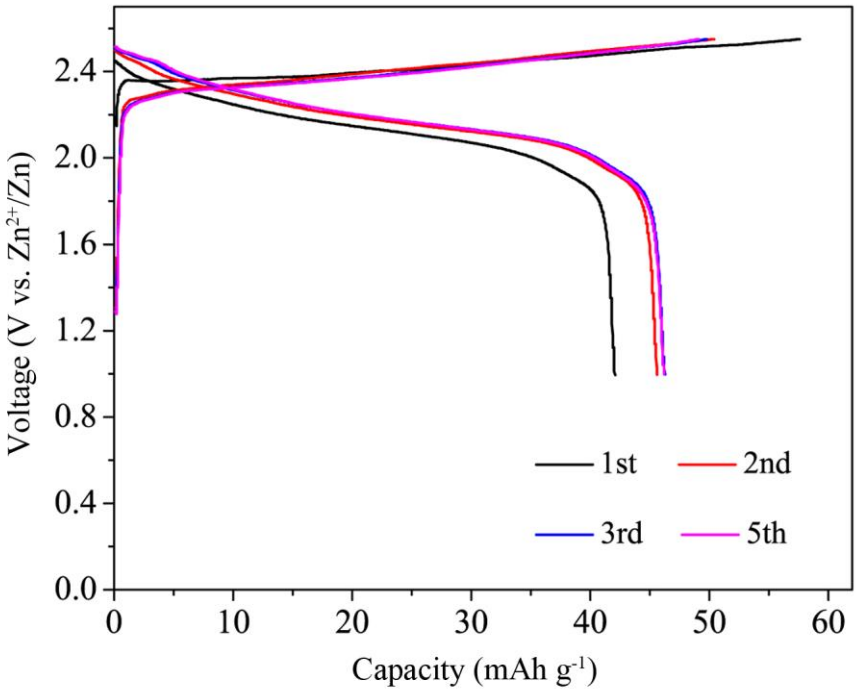

Figure S13. Typical charge/discharge curves of the graphite cathode using stainless steel foil as the current collector at 50 mA g^{-1}.

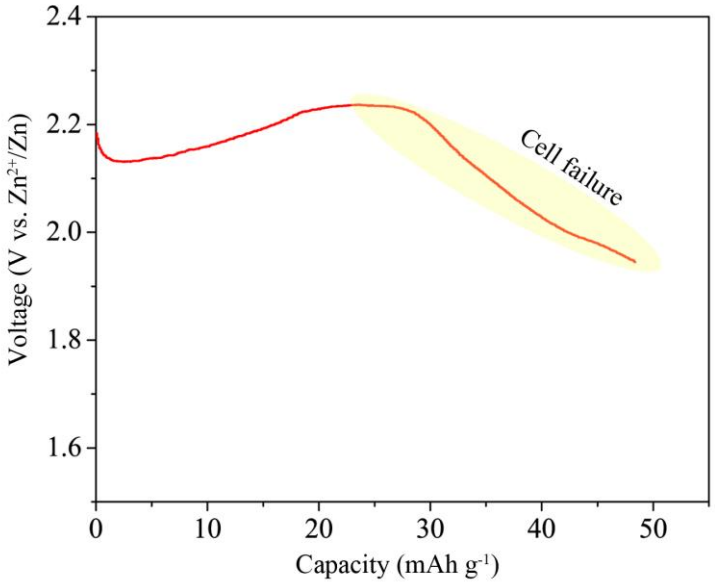

Figure S14. Charge curve of the Zn-graphite battery using the 1 M $Zn(TFSI)_2$ in EC/DEC electrolyte at 50 mA g^{-1}.

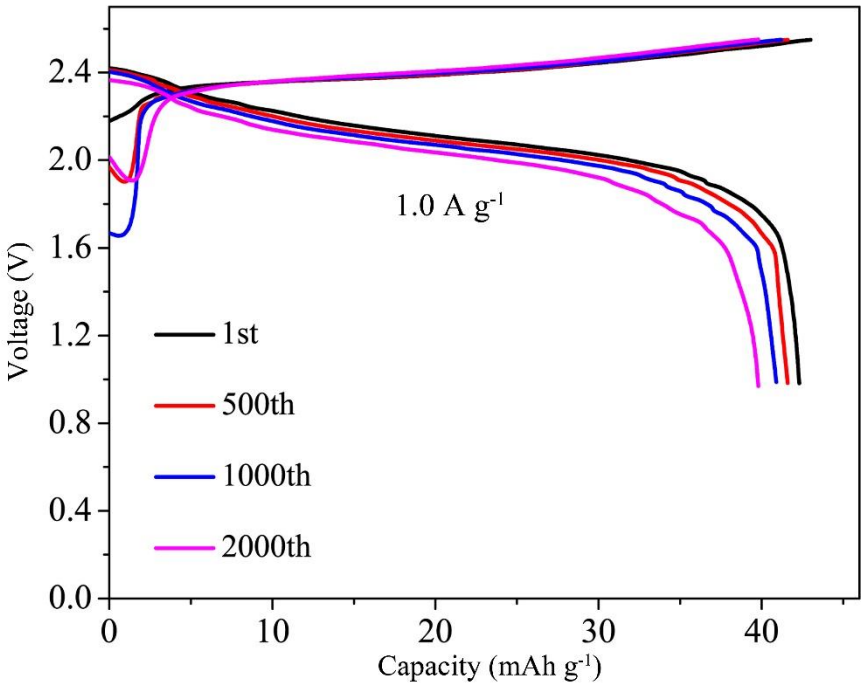

Figure S15. Representative charge/discharge profiles of the Zn-graphite battery at 1.0 A g^{-1}.

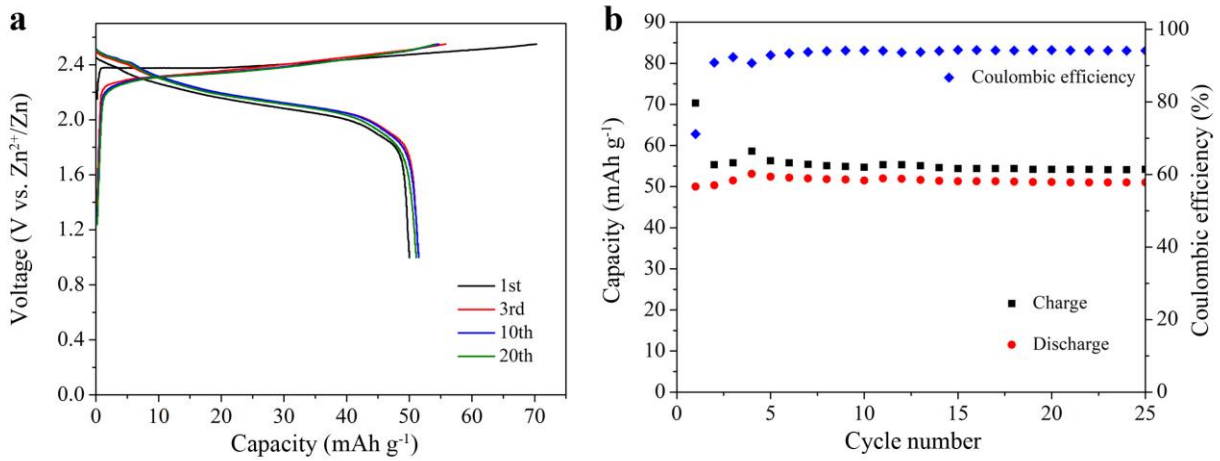

Figure S16. (a) Typical charge/discharge curves and (b) cycling performance of the graphite cathode with a lower loading mass of ~2 mg cm^{-2} at 50 mA g^{-1}.

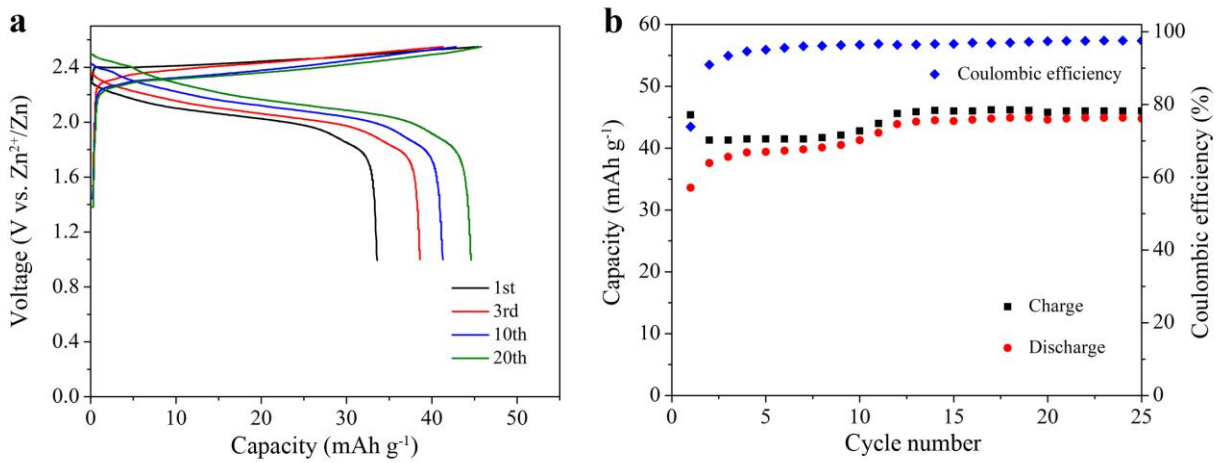

Figure S17. (a) Typical charge/discharge curves and (b) cycling performance of the graphite cathode with a higher loading mass of ~10 mg cm^{-2} at 50 mA g^{-1}.

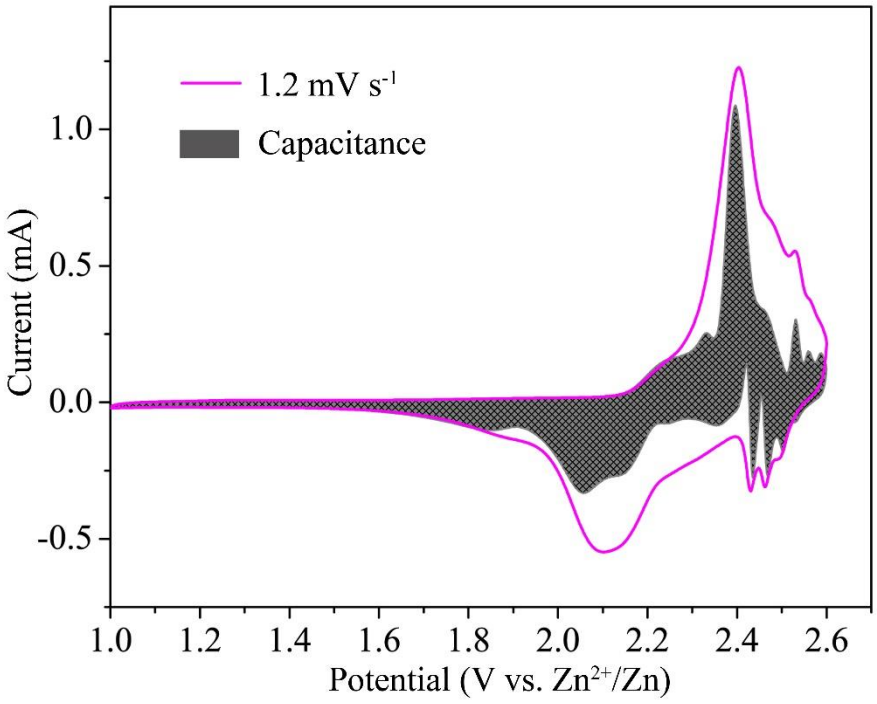

Figure S18. CV profile of the graphite cathode displaying the pseudocapacitive contribution (grey region) to the total current at 1.2 mV s^{-1}.

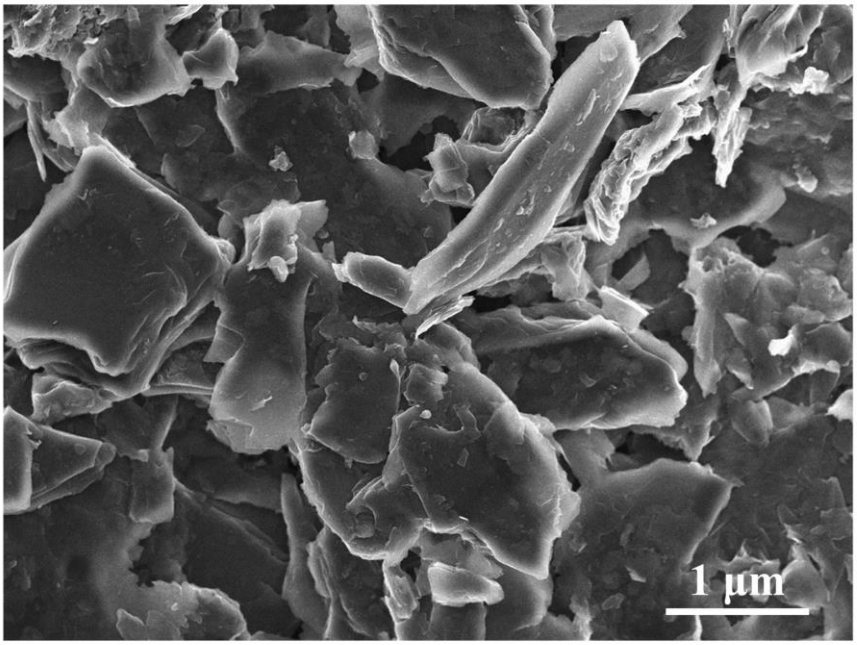

Figure S19. SEM image of the pristine graphite electrode.

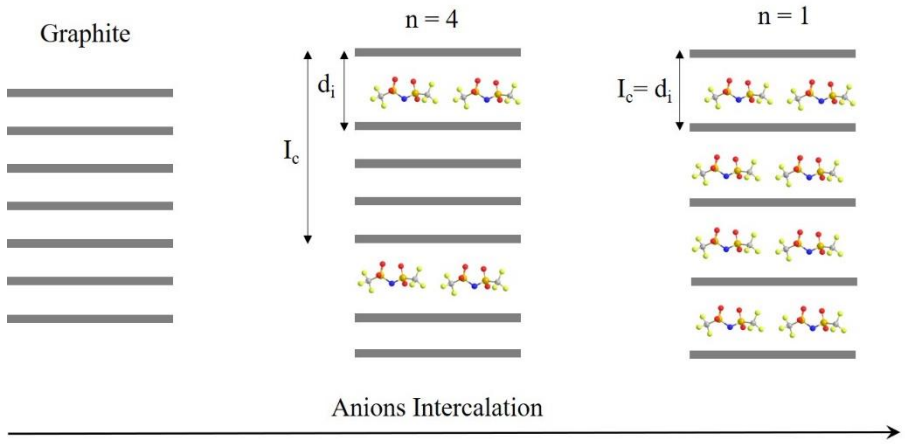

Figure S20. Schematic diagram of the selected stages of graphite intercalation compounds (GIC). I_c is the periodic distance. d_i is the intercalant gallery height.

According to the Bragg's law,

$d_{(00n+1)} = \lambda/2\sin\theta_{(00n+1)} = I_c/n+1$ (Equation S1);

$d_{(00n+2)} = \lambda/2\sin\theta_{(00n+2)} = I_c/n+2$ (Equation S2)

By determining the ratio of the d(00*n*+1)/d(00*n*+2) peak position, the most dominant state n can be assigned as follow:

$n = 1/(\sin\theta_{(00n+2)}/\sin\theta_{(00n+1)} - 1) - 1$ (Equation S3)

After assigning the (00*n*+1) indices, the intercalant gallery height (d_i) and gallery expansion (Δd) can be calculated using:

$I_c = d_i + (n-1) \times 3.35\ \text{Å} = \Delta d + 3.35\ \text{Å} \times n = (n+1) \times d_{(00n+1)}$ (Equation S4)[1-3]

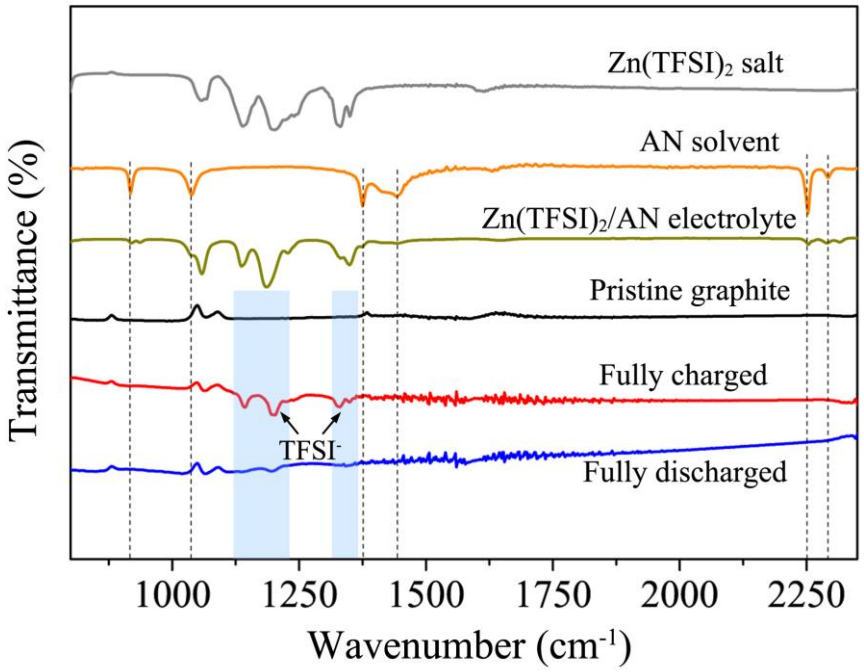

Figure S21. FTIR spectra of the $Zn(TFSI)_2$ salt, AN solvent, $Zn(TFSI)_2$/AN electrolyte, pristine graphite cathode, and graphite cathodes at the fully charged and discharged states.

Obviously, the charged graphite shows the intercalated $TFSI^-$ signals between 1125 cm^{-1} and 1375 cm^{-1}, and no AN vibration peaks can be observed, further attesting that no solvent co-intercalation occurs. Moreover, the two main peaks of $TFSI^-$ display blue shift from 1137 cm^{-1} and 1187 cm^{-1} in the $Zn(TFSI)_2$/AN electrolyte to 1143 cm^{-1} and 1200 cm^{-1} in the charged cathode, may due to the different absorbance nature of $TFSI^-$ in AN solvents and in graphite interlayers. After discharging, the signal of graphite can revert to the pristine state, associated with the anions deintercalation.

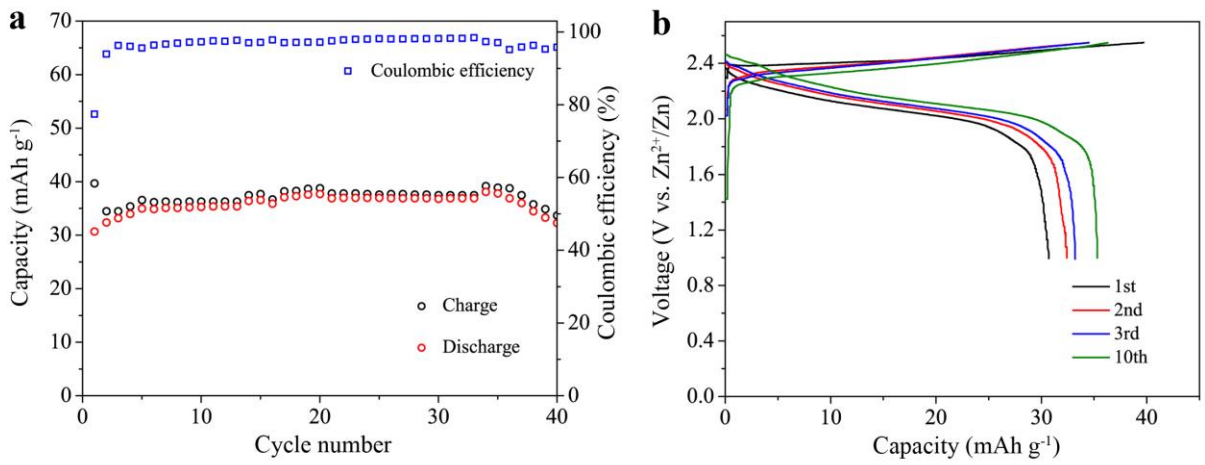

Figure S22. (a) Cycling performance and (b) typical charge/discharge curves of the Ti-graphite cell in 1 M $Zn(TFSI)_2$/AN electrolyte at 50 mA g^{-1}.

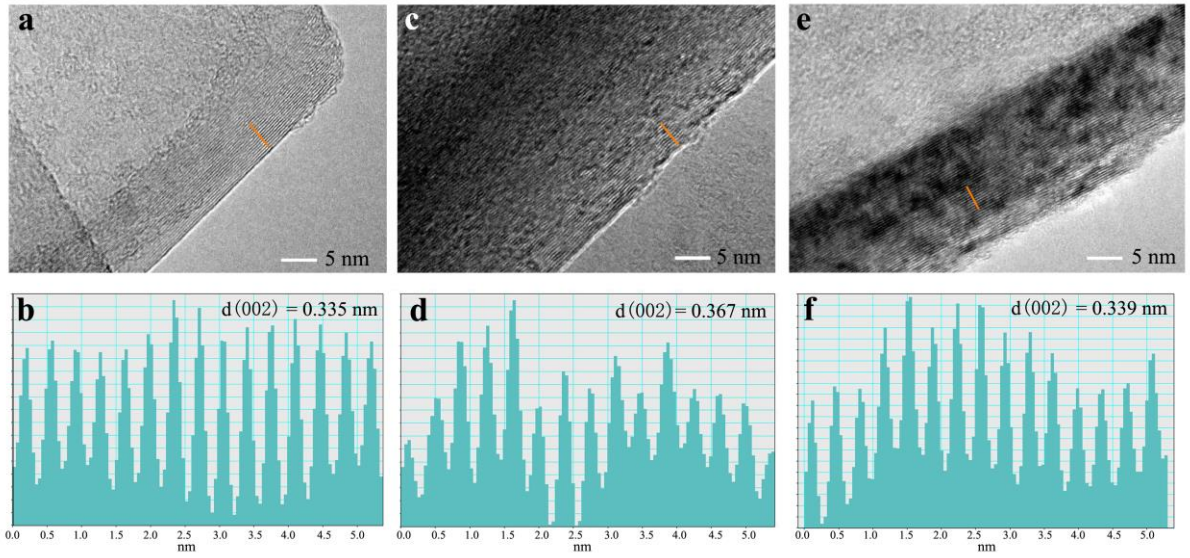

Figure S23. (a,c,e) HRTEM images and (b,d,f) the contrast profiles along the orange lines of the (a,b) pristine graphite, and graphite cathodes at the first fully (c,d) charged and (e,f) discharged states.

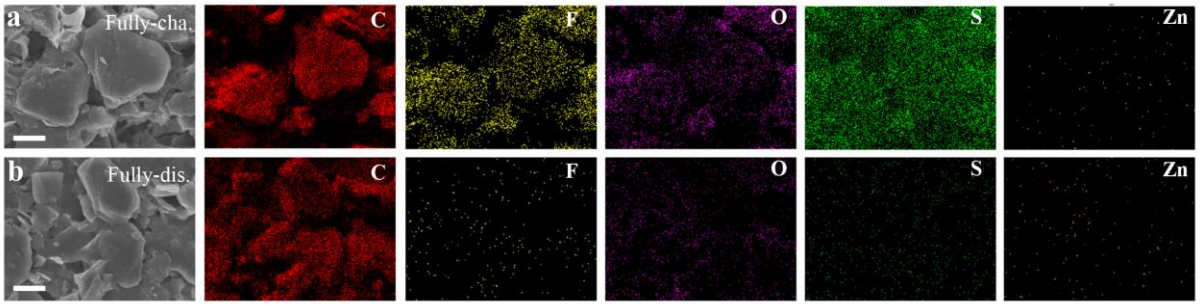

Figure S24. SEM images of the first fully (a) charged and (b) discharged graphite cathodes along with the relevant element mapping images.

Supplementary Note 1

Calculation of the ratio of electrolyte for anion intercalation in the cycle test to the total amount of electrolyte addition.

The 1 M $Zn(TFSI)_2$/AN electrolyte added in one coin-type cell is 60 μL, corresponding to 0.12×10^{-3} mol $TFSI^-$ anions. The loading mass of graphite is 4 mg cm^{-2} and the area of current collector is 0.785 cm^2 (round slice with a diameter of 1 cm). Thus, the graphite mass is 3.14 mg in one cell. In Figure 2b, the stable specific charge capacity is 50 mAh g^{-1} (the 10th cycle) at 0.05 A g^{-1}, corresponding to 0.157 mAh total capacity ($50 \times 3.14 \div 1000 = 0.157$ mAh) that is 0.5652 Coulomb (C) or 0.5858×10^{-5} mol e^- ($0.157 \times 3.6 = 0.5652$ C; 1 C = 1.0365×10^{-5} mol e^-). According to the equation of x $TFSI^-$ + Graphite ↔ Graphite$[TFSI^-]_x$ + x e^-, the charge process will consume 0.5858×10^{-5} mol $TFSI^-$ anions. Therefore, the ratio of electrolyte for anion intercalation in the 10th cycle to the total amount of electrolyte addition can be estimated to ~4.88% ($0.5858 \times 10^{-5} \div (0.12 \times 10^{-3}) \times 100\% = 4.88\%$). Similarly, the charge capacity is 42.7 mAh g^{-1} at 1.0 A g^{-1} in Figure 2e, and the corresponding ratio can be estimated to ~4.17%.

Table S1. Electrochemical performances of the multivalent cations (e.g., Ca^{2+}, Al^{3+}) based batteries using graphite as cathodes.

Battery Systems	**Electrolyte**	**Electrochemical Performance**	**Ref.**
Al-graphite battery using Al foil anode and graphitic foam cathode	$AlCl_3$/1-ethyl-3-methylimidazolium chloride ([EMIm]Cl) ionic liquid electrolyte	65 mAh g^{-1} at 0.066 A g^{-1}; ~90% CE at 0.1 A g^{-1}; ~100% capacity retention after 4000 cycles at 4.0 A g^{-1} with CE values between 90% and 97%.	1
Al-graphite dual-ion battery using Al foil anode and graphite cathode	4 M $LiPF_6$ ethyl–methyl carbonate (EMC) electrolyte	78 mAh g^{-1} at 0.5 A g^{-1}; ~75% CE at 0.05 A g^{-1}; ~75% capacity retention when the current density increased from 0.1 to 0.5 A g^{-1}; ~88% capacity retention after 200 cycles at 0.2 A g^{-1} with CE values between 78% and 98%.	4
Ca-ion battery using Sn foil anode and graphite cathode	0.8 M $Ca(PF_6)_2$ in mixed solvents of EC-PC-DMC-EMC (volume ratio is 2:2:3:3)	45 mAh g^{-1} at 0.4 A g^{-1}; ~80% CE at 0.1 A g^{-1}; ~55% capacity retention when the current density increased from 0.1 to 0.4 A g^{-1}; ~95% capacity retention after 350 cycles at 0.1 A g^{-1} with CE values between 80% and 95%.	5
Ca-ion battery using mesocarbon microbead anode and expanded graphite cathode	0.7 M $Ca(PF_6)_2$ in mixed solvents of EC-DMC-EMC (volume ratio is 4:3:2)	~83% capacity retention when the current density increased from 1 C to 5 C; 62 mAh g^{-1} at 1 C with 94% capacity retention after 300 cycles with CE values between 60% and 92%.	6
Zn-graphite battery using Zn foil anode and commercial graphite cathode.	1 M $Zn(TFSI)_2$ in AN	47.5 mAh g^{-1} at 0.05 A g^{-1} 42.3 mAh g^{-1} at 0.5 A g^{-1}; ~95% CE at 0.05 A g^{-1}; ~99% and 84% capacity retentions when the current density increased from 0.1 to 1.0 and to 4.0 A g^{-1}, respectively; 97.3% and 82% capacity retentions after 1000 and 4000 cycles at 1.0 A g^{-1} with CE values of ~100%.	This work

Supplementary References

[1] Lin, M.-C.; Gong, M.; Lu, B.; Wu, Y.; Wang, D.-Y.; Guan, M.; Angell, M.; Chen, C.; Yang, J.; Hwang, B.-J.; Dai, H. An Ultrafast Rechargeable Aluminium-Ion Battery. *Nature* **2015**, *520*, 324–328.

[2] Jiang, X.; Liu, X.; Zeng, Z.; Xiao, L.; Ai, X.; Yang, H.; Cao, Y. A Nonflammable Na^+-Based Dual-Carbon Battery with Low-Cost, High Voltage, and Long Cycle Life. *Adv. Energy Mater.* **2018**, *8*, 1802176.

[3] Kravchyk, K. V.; Bhauriyal, P.; Piveteau, L.; Guntlin, C. P.; Pathak, B.; Kovalenko, M. V. High-Energy-Density Dual-Ion Battery for Stationary Storage of Electricity Using Concentrated Potassium Fluorosulfonylimide. *Nat. Commun.* **2018**, *9*, 4469.

[4] Zhang, X.; Tang, Y.; Zhang, F.; Lee, C.-S. A Novel Aluminum-Graphite Dual-Ion Battery. *Adv. Energy Mater.* **2016**, *6*, 1502588.

[5] Wang, M.; Jiang, C.; Zhang, S.; Song, X.; Tang, Y.; Cheng, H.-M. Reversible Calcium Alloying Enables a Practical Room-Temperature Rechargeable Calcium-Ion Battery with a High Discharge Voltage. *Nat. Chem.* **2018**, *10*, 667–672.

[6] Wu, S.; Zhang, F.; Tang, Y. A Novel Calcium-Ion Battery Based on Dual-Carbon Configuration with High Working Voltage and Long Cycling Life. *Adv. Sci.* **2018**, *5*, 1701082.